

DFT-based designed surface functionalized carbon black for electrochemical detection of Arsenic and its experimental validation

Aneeqa Batool ^{a,1}, Sana Qureshi ^{a,1}, Arslan Ahmad ^a, Shaista Zubaid ^{a,b}, Laraib Saeed ^a, Khurshid Ayub ^a, Tahir Rasheed ^c, Tauqir A. Sherazi ^{a,2,*}

^a Department of Chemistry, COMSATS University Islamabad, Abbottabad Campus, Abbottabad 22060, Pakistan

^b Department of Chemistry, Abbottabad University of Science and Technology, Abbottabad, Pakistan

^c Interdisciplinary Research Center for Advanced Materials, King Fahd University of Petroleum & Minerals (KFUPM), Dhahran, 31261, Saudi Arabia



ARTICLE INFO

Keywords:

Electrochemical sensors
DFT studies
Arsenic
Cyclic voltammetry
Square wave anodic voltammetry

ABSTRACT

Carbon-based materials are cost-effective and eco-friendly but have limited sensitivity for detecting heavy metals. Density Functional Theory (DFT) is employed to design materials suitable for sensing, based on their interaction with analytes. Oxidized carbon black embedded with silver nanoparticles (OCB-Ag) is designed and studied via DFT, showing promising conductivity and arsenic interaction. Experimental validation confirmed its efficacy. The OCB-Ag nanocomposite was synthesized via in-situ preparation and used as an electrode material for arsenic detection. Characterization via UV-Visible spectroscopy and X-ray diffraction confirmed successful synthesis. Electrochemical interaction with arsenite was studied using square wave anodic stripping voltammetry. The OCB-Ag platform exhibited a linear current response up to 600 ppm of As³⁺, with a low limit of detection (0.01 ppm) and good sensitivity (5.9 μA ppm⁻¹). The detection limit of electrode material for As³⁺ lies within the threshold value set by world health organization for drinking water. The experimental results validated the concept of designing electrochemical sensing platform through DFT, and its potential for detection of As³⁺.

1. Introduction

Arsenic contamination, whether in organic or inorganic form, poses a significant global challenge [1]. Arsenic exists in various oxidation states, including -3, 0, +3, and +5, and out of these the arsenite As (III) and arsenate As (V) are the most stable ones [2]. These both forms are extremely hazardous, and more particularly As (III) is several times more poisonous than As (V) [3]. The long-term exposure to As (III) can cause a number of health problems, such as cancer, heart diseases, and skin sores [4,5]. The World Health Organization have set the permissible level of arsenic contamination in drinking water at 0.01 ppm or 10 ppb [6]. Arsenic enters the body through ingestion and is absorbed by the intestinal tract. It then interacts with phosphate groups within the body, displacing them and leading to various abnormalities [6,7]. Therefore, it is crucial to detect arsenic contamination particularly As (III). Several analytical techniques are available for arsenic detection, including fluorescence spectroscopy (FS), mass spectrometry (MS), Inductively

coupled plasma mass spectrometry (ICP-MS) and high-performance liquid chromatography (HPLC). However, these techniques have certain limitations such as high operating costs, complexity, and low sensitivity and selectivity [8]. Moreover, these are not easily accessible or portable. To overcome these challenges, electrochemical detection procedures offer number of advantages including cost-effectiveness, time efficiency, enhanced sensitivity, catalytic performance, repeatability, and straightforward implementations in the lab as well as in the fields [9,10].

The electrochemical procedures involving cyclic voltammetry and square wave anodic stripping voltammetry (SWASV) are suitable techniques performed to identify the presence of As³⁺ in aqueous solution [10]. SWASV is an electrochemical technique combination of square wave voltammetry (SWV) and anodic stripping voltammetry (ASV). SWV offers lower limit of detection compared to cyclic voltammetry or amperometry. In SWV analysis, potential is varied as a square wave superimposed on a linear sweep and the current is measured after each

* Corresponding author.

E-mail address: sherazi@cuiatd.edu.pk (T.A. Sherazi).

¹ These authors contributed equally.

² Visiting affiliation: INM, Leibniz Institute for New Materials, Campus D2.2, 66123 Saarbrücken, Germany.

potential pulse [11,12]. Anodic stripping voltammetry (ASV) analysis involves two steps: preconcentration of the metal cations to be detected where metal cations are reduced to zero-valent state on the electrode surface followed by their redissolution through oxidation. This oxidation response is characterized by a peak observed in the applied potential range, and its position is the characteristic of each metal atom [13].

The electrochemical detection of As^{3+} has already been studied using platinum disk electrode, gold film, Au/GO nanocomposites, and silver, etc., as working electrodes [14]. Some other types of materials such as metal oxides & sulfides, titanates, phosphides, carbon-based material, or hybrid nanocomposites are also used for sensing applications [15,16]. The nanomaterials forming composites with noble metallic nanoparticles (Au, Pt, Pd, Ag, and different bimetallic nanoparticles) are also applicable for detection of As (III) due to their unique optical, electrical, and electrochemical properties [17,18]. Among the various metallic nanoparticles, silver nanoparticles (AgNPs) offer themselves as a desirable for the preparation of photocatalyst and preparation of chemically modified electrodes for electrochemical sensing due to its high quantum characteristics of small granule diameter, high conductivity, large specific surface area, cost effective, and stability [19,20].

Carbon black is a readily available, cost effective, and biocompatible material, which also exhibit interesting and excellent electrical, optical, chemical, and electronic properties [21,22]. Thus, considered as potential substrate material to develop sustainable and cost-effective sensing platform. The carbon black, once transformed into oxygenated carbon black (OCB), includes functional groups containing oxygen, such as hydroxyl (-OH), and carbonyl (C = O) groups. These covalent oxygen functional groups in OCB give rise to possibility to interact this system with other species, which could be translated into molecular-level chemical or electrochemical sensing device [23].

The interaction between the analyte and the sensing platform plays a vital role in electrochemical sensing. So, it is of interest to understand and design the sensing platform theoretically, which proves the interacting capability between itself and the analyte. This could help to save time, energy, and additionally environment could also be protected using the least amount of chemicals taking theoretical conceptualization in account before performing experiments [24]. The Density Functional Theory (DFT) calculations give an estimation of the interaction mechanism, and important interaction parameters including bond length and interaction energy [25]. DFT studies play a vital role throughout various stages of the sensing processes. It helps in the selection of a suitable base material for sensing application, its modification to improve the sensing capability, and also suggests the nature of interactions between sensing platform and analyte [26].

In the present work, silver embedded OCB was designed through DFT studies as an active electrochemical sensing platform for arsenic detection and the theoretical findings are validation through experimental approach and the sensing performance was determined through anodic stripping voltammetry. A low-cost and facile approach for OCB-Ag composite formation is reported in which simultaneous in-situ preparation and incorporation of Ag nanoparticles within the OCB surface occurs. The synthesis was conducted in an aqueous solution, which is a versatile and environmentally friendly process. The OCB-Ag is readily dispersed into water and common organic solvents to form a stable suspension without any additional protection by polymeric or surfactant stabilizers. The OCB-Ag composite was directly deposited onto the glassy carbon electrode for electrochemical detection and quantification of arsenic.

2. Materials and methods

2.1. Computational methodology

All structures are optimized by using Gaussian 9 package [27], while for visualization purpose Gauss View 5.0 is used. Standard DFT

functional B3LYP along with basis set 6–31G(d, p) for H, C, and O atoms, whereas basis set SDD for Ag and As atoms were used. B3LYP/6–31G(d, p) level of theory is used to evaluate the electronic properties based on the well reported reliability and accuracy of these levels [28]. Electronic properties are also calculated at B3LYP/6–31G(d, p) level for OCB and B3LYP/6–31G(d, p)/SDD level for the complexes involving heavy atoms. The transition metals exhibit variable multiplicities to acquire the most stable spin states. Thus, the optimization of silver and arsenic atoms was done at different spin states such as doublet, quartet, and sextet. These optimizations study concluded that the doublet is the most stable state for both Ag and As. The interaction energies of OCB-Ag and As@OCB-Ag were calculated by using the following equation.

$$\text{Interaction energy (OCB - Ag)} = E_{\text{OCB-Ag}} - (E_{\text{OCB}} + E_{\text{Ag}}) \quad (1)$$

$$\text{Interaction energy (As@OCB - Ag)} = E_{\text{As@OCB-Ag}} - (E_{\text{OCB-Ag}} + E_{\text{As}}) \quad (2)$$

Frontier molecular orbital (FMO) analysis, Natural bond Orbital (NBO), density of states (DOS), and electron density difference (EDD) analysis were also performed. The density of states (DOS) and electron density difference (EDD) are generated through Multiwfn [29] and VMD [30] software.

2.2. Experimental methodology

2.2.1. Chemicals

All the chemicals and reagents were of analytical grades and used without any purification. Silver nitrate (AgNO_3 , 98 %), Arsenic trioxide (As_2O_3 , 99 %), Ammonium persulfate ($(\text{NH}_4)_2\text{S}_2\text{O}_8$, 99.5 %), Cobalt chloride (CoCl_2), Zinc Chloride (ZnCl_2), Cadmium Sulphate (CdSO_4), Iron Chloride (FeCl_3), copper sulphate (CuSO_4), Potassium Chloride (KCl), and Sodium hydroxide (NaOH , 99 %) were purchased from Sigma Aldrich. Carbon black and Iron cyanide $\text{Fe}(\text{CN})_2$ was purchased from Alpha-Aesar, Trisodium citrate ($\text{Na}_3\text{C}_6\text{H}_5\text{O}_7$, 99 %), Hydrochloric acid (HCl , 37 %) and Nitric acid (HNO_3 , 70 %) was purchased from Daejung Co., Ltd.

2.2.2. Synthesis of oxidized carbon black

The oxidation of Carbon black (CB) was performed by using saturated solution of $(\text{NH}_4)_2\text{S}_2\text{O}_8$ as an oxidizing agent as reported in our previous work [31]. The saturated solution of ammonium persulfate is prepared by adding 37 g of oxidant to the 100 mL of 4 N H_2SO_4 solution. The CB (3% w/v) was then added to $(\text{NH}_4)_2\text{S}_2\text{O}_8$ solution in round bottom flask fitted with a magnetic stirrer. The mixture was allowed to stir for 48 h at 30 °C to complete the oxidation of carbon black. The oxidized carbon black (OCB) was washed with DI water several times and then dried at 80 °C under vacuum.

2.2.3. Synthesis of silver nanoparticles

The synthesis of silver nanoparticles was performed by dissolving 5 mg of AgNO_3 in 20 mL of deionized water and heated until it started boiling (100 °C), then 1 %, and 2 % trisodium citrate were added in different reaction mixtures to check the effect of concentration on the size and surface potential of the Ag nanoparticles. The temperature of reaction mixture was maintained at 100 °C for 30 min until yellow color solution of silver nanoparticles was obtained. The obtained sample of AgNPs prepared with 1 % trisodium citrate and with 2 % trisodium citrate were labelled as AgNP.1 and AgNP.2, respectively.

2.2.4. In-situ synthesis of OCB-Ag nanocomposite

To prepare the OCB-Ag nanocomposite, the dispersion of oxidized carbon black and silver nitrate solution were prepared separately. The OCB dispersion was prepared by adding 100 mg of oxygenated carbon black in 80 mL deionized water and ultrasonicated for 1 hour. The solution of silver nitrate was prepared by dissolving 5 mg of AgNO_3 into 20

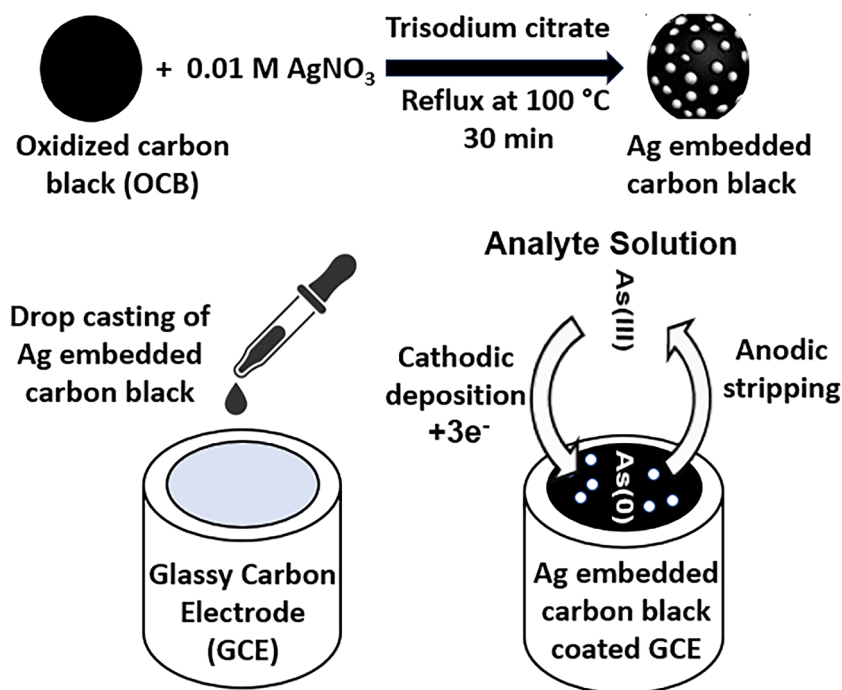


Fig. 1. Scheme of Ag embedded oxidized carbon black synthesis and electrode fabrication.

mL of deionized water. Afterwards, these two solutions were mixed with each other and heated with constant stirring until temperature reached to 100 °C. At this point, 1 mL of 1 % trisodium citrate solution was added in the reaction mixture. The temperature of the reaction mixture was maintained at 100 °C for the next 30 min. The obtain mixture was centrifuge at 8000 rpm to obtain OCB-Ag, which dried at 90 °C under vacuum for 5 h. The sample obtained was labelled as OCB-Ag.1 with 1 % trisodium citrate. The exact same procedure was adopted to prepare OCB-Ag.2 by just replacing 1 % trisodium citrate with 2 % trisodium citrate.

2.3. Preparation of OCB-Ag/GCE

The electrochemical analysis of prepared composite material was performed by using Glassy carbon electrode as working electrode. The prepared sensing material, OCB-Ag was deposited on the surface of glassy carbon electrode. However, before the deposition it is important to polish the glassy carbon electrode, so it was done by using 0.05 mm alumina slurry on polishing cloth. A small amount of alumina was placed on polishing cloth then a few drops of DI water were added to make alumina slurry. The electrode was rotated in form of digit 8 so it is

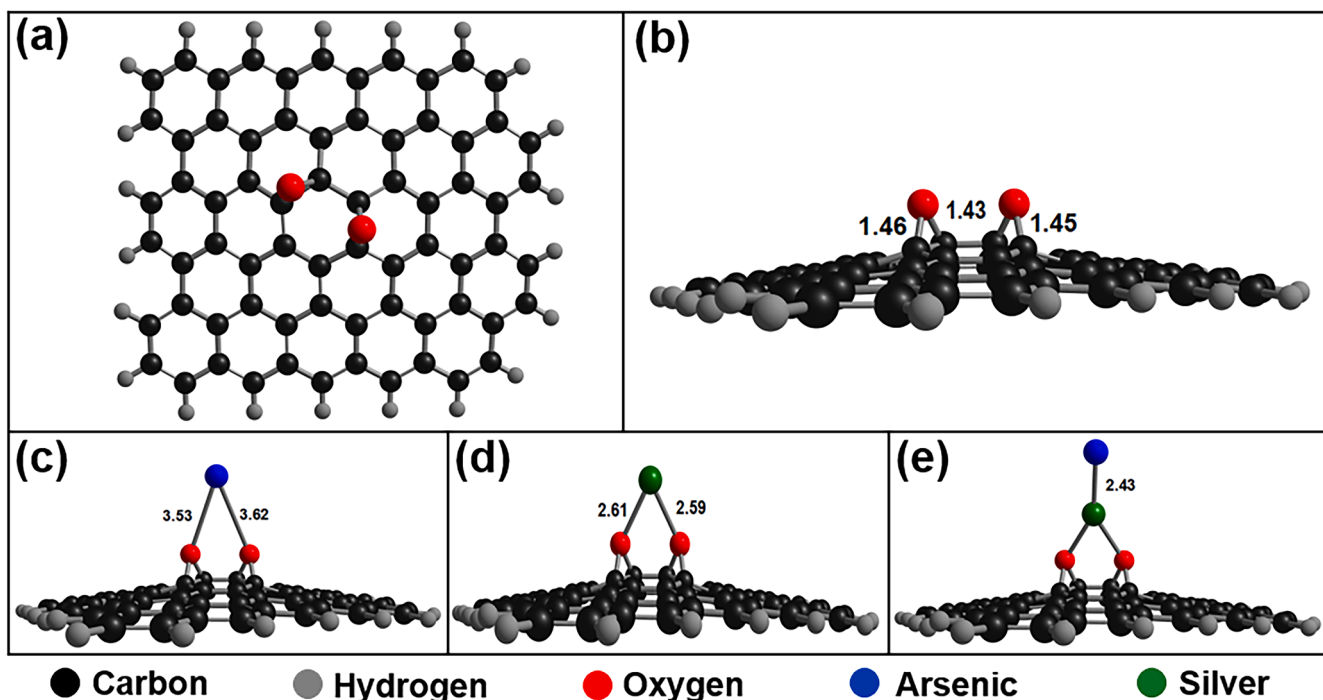


Fig. 2. Optimized structures of all the complexes, (a) top view of OCB, (b) side view of OCB, (c) As@OCB, (d) OCB-Ag, and (e) As@OCB-Ag.

Table 1

Bond lengths, Interaction Energies, HOMO-LUMO energies, Energy gaps E_{H-L} , Q_{NBO} values in each active surface before and after interaction with analyte.

System	Bond length (Å)	E_{int} (eV)	HOMO (eV)	LUMO (eV)	E_{H-L} (eV)	$Q_{NBO} e $
OCB	—	—	-3.91	-3.40	0.51	—
As@OCB	3.62	0.01	-4.67	-2.91	1.76	0.02
OCB-Ag	2.61	0.79	-4.42	-2.74	1.69	0.05
As@OCB-Ag	2.43	-2.00	-4.00	-3.55	0.45	0.16

clean from every angle. The electrode was placed in DI water and sonicated for 2 min. The 5 mg of composite (OCB-Ag) was then added to 2.5 mL of DMF (dimethyl formamide) and 40 μ L of 5 % nafion (binder). The above mixture sonicated for 30 min until stable suspension was formed. The prepared suspension was then deposited on the surface of glassy carbon electrode by using 10 μ L of suspension and dropped it by drop casting method. The schematic diagram for the preparation of OCB-Ag and electrode fabrication is presented in Fig. 1.

2.4. Characterization and electrochemical studies

The Dynamic light scattering (DLS) analysis (size & Zeta-potential) was performed on Zeta-sizer Nano (model ZSP Malvern Analytical technology, UK), by using software Malvern Zeta-sizer. All the samples for analysis were prepared in deionized (DI) water and sonicated 10 min before analysis, and all the measurements were taken in triplicate at 25 °C as set temperature. The UV–Visible spectra were obtained by using A Shimadzu UV-1700 UV–Visible spectrophotometer with a wavelength range of 190–1100 nm, equipped with tungsten and deuterium lamp. The X-ray diffraction (XRD) analysis was performed to determine the crystal structure of the samples and phase changes using Bruker D8 advance XRD equipped with 1D detector (Bragg Brentano) and analysis software including TOPAS for Rietveld and EVA & MATCH for

phase analysis. Scanning electron microscopy (SEM) and energy dispersive spectroscopy (EDS) were conducted by using JEOL SEM jsm7500F Cold field-emission scanning electron microscope equipped with SE & amp; BSE detectors in Oxford EDS system. The solution was made at room temperature and sonicated for 10 min before analysis. All electrochemical studies were performed with the Gamry 3000 electrochemical workstation. The conventional three-electrode system was utilized. The working electrode used was a bare or modified glassy carbon electrode (GCE, 3 mm in diameter), the auxiliary and reference electrodes were platinum wire and Ag/AgCl, respectively. Electrochemical impedance measurements were performed in 0.1 M KCl containing 1.0 mM $Fe(CN)_6K_3$ (1: 1 mixture).

3. Result and discussion

3.1. Structural optimization and interaction energies

The optimized structure of OCB is presented in Fig. 2(a) (top view) and 2(b) (side view). The oxidation of carbon black can induce different functional groups such as epoxy, hydroxyl, and carbonyl groups, etc. For the sake of simplicity, we consider a single layered carbon sheet as carbon black, and the epoxy group as a functional group resulting from oxidation. The choice of exopy group at the carbon sheet as representative of oxidized carbon black is supported by reported literature [32]. The two epoxy groups can be placed on the six-membered ring in three different ways (ortho-, meta-, and para-positions).

The structural optimization calculations indicated that the carbon structure with epoxy groups at meta-position to each other is the most stable structure. The bond length of C–O bond (1.45 Å) in the optimized OCB is in line with already reported literature [32]. The optimized structures of OCB, As@OCB, OCB-Ag, and As@OCB-Ag are presented in Fig. 2(a-e). The stability of complexes was assessed by examining the interaction energy (E_{int}), as reported in Table 1.

A higher interaction energy indicated a greater degree of stability of

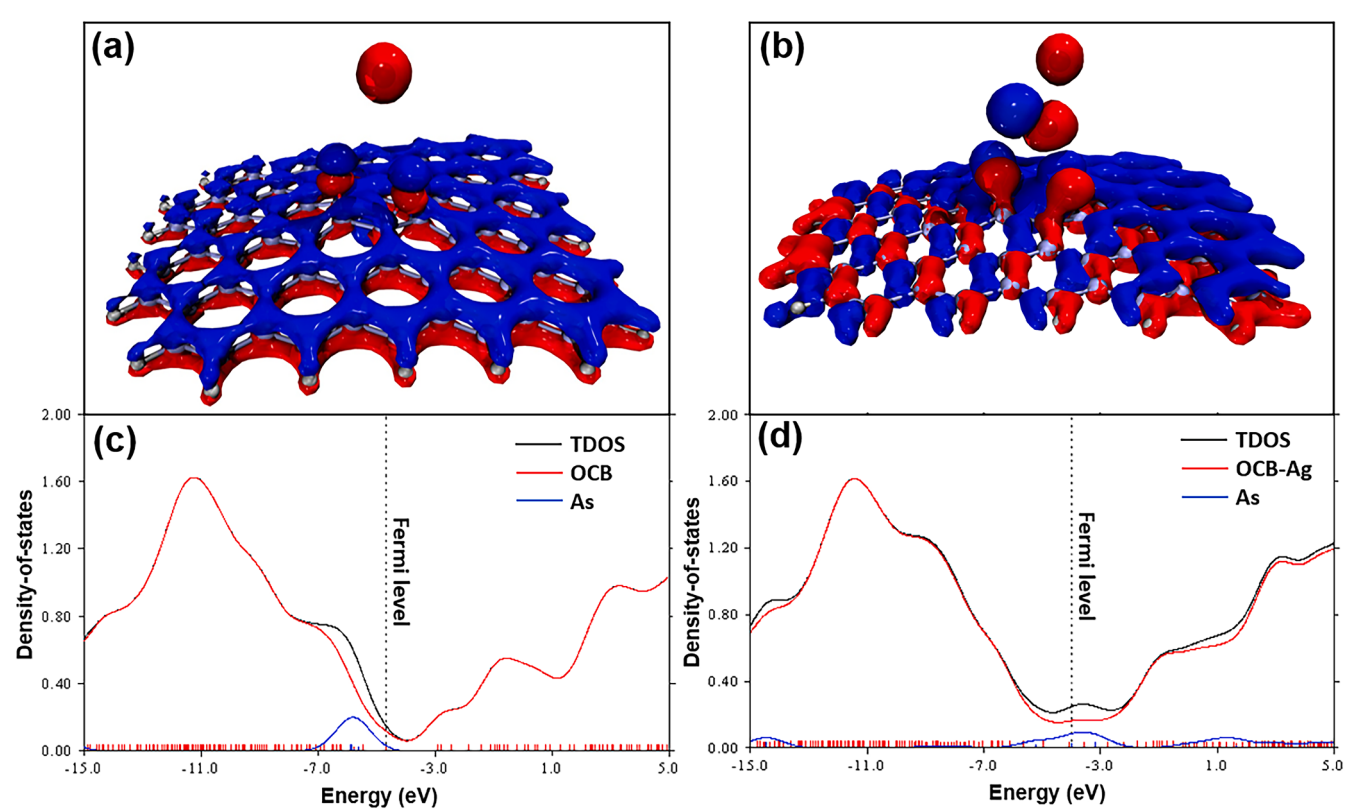


Fig. 3. Electronic properties of As@OCB and As@OCB-Ag, (a) EDD of As@OCB, (b) EDD of As@OCB-Ag, (c) DOS of As@OCB, and (d) DOS of As@OCB-Ag.

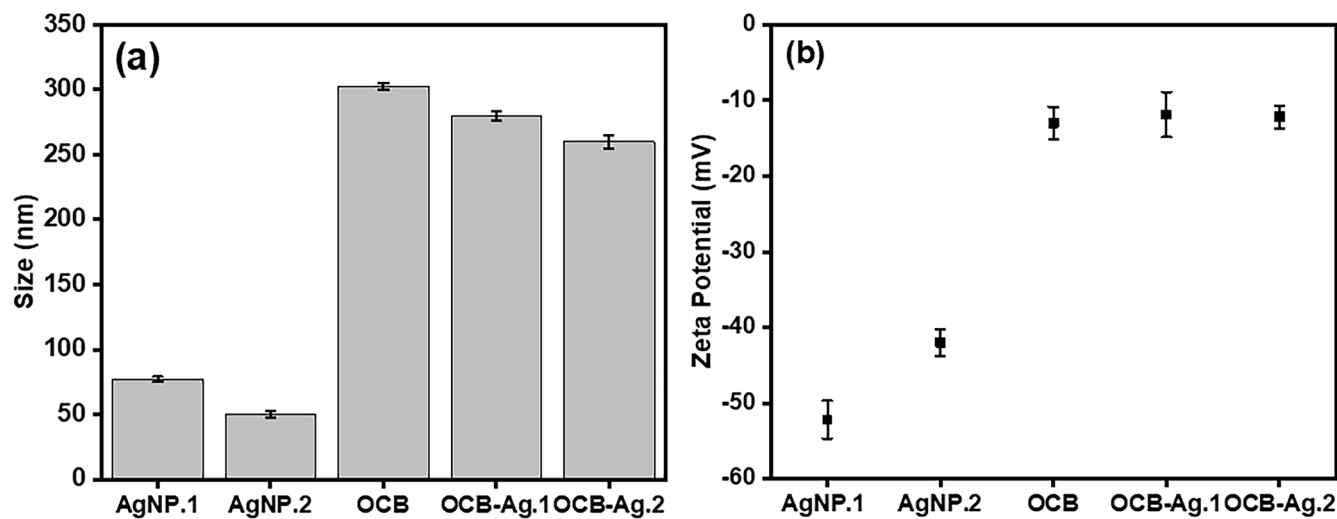


Fig. 4. DLS size distribution (a) and Zeta potentials (b) of Ag nanoparticles prepared by 1 % trisodium citrate (AgNP.1) and 2 % trisodium citrate (AgNP.2), OCB, and composite of OCB with AgNP.1 (OCB-Ag.1), and composite of OCB with AgNP.2 (OCB-Ag.2). (Error bars are based on measurement of each sample in triplicate).

the resulting complex. The lowest interaction energy is observed for As@OCB while the highest interaction is observed for As@OCB-Ag. This observation suggested that sensitivity of OCB towards As is significantly increased after depositing Ag onto it. The interaction energy between OCB and Ag is positive, indicating lack of chemical affinity between both the components. The interaction energy suggested that the composite formation between OCB and Ag is a physical binding of both components originated during the insitu formation of silver nanoparticle supported by heating process as reported in the following experimental validation section of this article [33].

The adsorption of arsenic on the sensing platform surfaces (OCB and OCB-Ag) induces a significant change in the electronic structure of these surfaces. To investigate the interaction between the analyte and the surface in terms of charge transfer, natural bond orbital (NBO) analysis and electron density difference (EDD) analysis were performed. The bond length between the analyte and sensing platform or just the distance between these two components in the optimized structures were determined that is found to be 3.62 Å and 2.43 Å for As@OCB and As@OCB-Ag complex, respectively. The shorter bond length observed in As@OCB-Ag is in line with a higher degree of charge transfer (0.16e) from the surface to the analyte as measured through NBO.

The EDD analysis of As@OCB is illustrated in Fig. 3(a), where oxygen being highly electronegative attracts electrons from the carbon sheet towards itself. Consequently, the carbon sheet exhibits an electron-depleted region (depicted in blue). The lone pairs of oxygen are hybridize with the LUMO orbitals of arsenic, facilitating the transfer of electrons to arsenic, with NBO charge of 0.02e. In the case of As@OCB-Ag, as shown in Fig. 3(b), the EDD analysis reveals an asymmetric distribution of the electron-depleted region over the sheet.

This asymmetry is due to the O-Ag-As functionalization over the carbon sheet, which tilts more towards one side, leading to a greater electron gain from that side. The net NBO charge transfer from the surface to the analyte is 0.16e, as mentioned in Table 1. The sensing capability of OCB-Ag is further assessed by examining electronic parameters, including frontier molecular orbitals (FMO), total density of states (TDOS) and partial density of states (PDOS). The FMO analysis enables us to understand the changes in electronic levels such as highest occupied molecular orbital (HOMO) and lowest unoccupied molecular orbital (LUMO) during interaction of analyte that is As with the sensing surface platform surface that are taken OCB and OCB-Ag. The calculated HOMO and LUMO energies and their corresponding energy gaps (E_{H-L}) are presented in Table 1. The decrease in magnitude of HOMO energy level and increase in magnitude of LUMO energy level represents the

shift toward fermi level, thus decreasing the band gap and vice versa. It is observed that the energy gap is increased, when arsenic is adsorbed on the bare OCB, suggesting its poor sensitivity for arsenic. However, the values of HOMO and LUMO energy levels for OCB-Ag experience a shift toward fermi level after As is placed onto it, thus decreasing the E_{H-L} , as reported in Table 1. The decreased E_{H-L} of As@OCB-Ag compared to OCB-Ag signifies enhanced conductivity and sensitivity of OCB-Ag towards arsenic which is consistent with the strong interaction energy (-2.00 eV) of arsenic over OCB-Ag. These findings theoretically proved that the Ag decoration on OCB enhances the sensing capability of arsenic as an analyte.

To gain further insights into the interactions and electronic behavior of interacting species, density of states (DOS) is investigated as presented in Fig. 3(c) and 3(d). The partial density of states (PDOS) provides information about the contribution of each species toward total density of states (TDOS). In the case of As@OCB as shown in Fig. 3(c), the PDOS of arsenic are near to fermi level therefore it could contribute to the total density of states at fermi level. However, the increase in the peak intensity of TDOS is minimal, suggesting a relatively weak interaction of arsenic with OCB. In contrast, in the case of As@OCB-Ag as shown in Fig. 3(d), it is observed that the intensity of TDOS at fermi level is increased when compared to OCB-Ag. This implies the generation of new energy levels which lies at higher energy than OCB-Ag. Thus, causing the increase in HOMO energy levels reducing the energy gaps which are consistent to the FMO analysis. The DOS analysis confirms that the addition of Ag to OCB enhances the sensing of arsenic by facilitating relatively stronger interactions and cause modification in the electronic structure of the surface that could potential detected by using electrochemical technique. Based on these assumptions supported by the DFT studies, experimental work is performed that validated the concept and the designed OCB-Ag provided interesting results in line with the theoretical calculations.

3.2. Experimental validation

Carbon black was modified into oxidized form and used for the detection of arsenic. The oxidized carbon black was used due to availability of active sites for the interaction with arsenic present in aqueous solution. The DLS studies are carried out to measure the hydrodynamic size and zeta potential of silver nanoparticles. Fig. 4(a) shows the hydrodynamic size of silver nanoparticles at different concentrations of 1 % and 2 % trisodium citrate, which is 78 nm and 50 nm. The size of OCB, OCB-Ag.1 and OCB-Ag.2 obtained as 308 nm, 227 nm, and 270 nm,

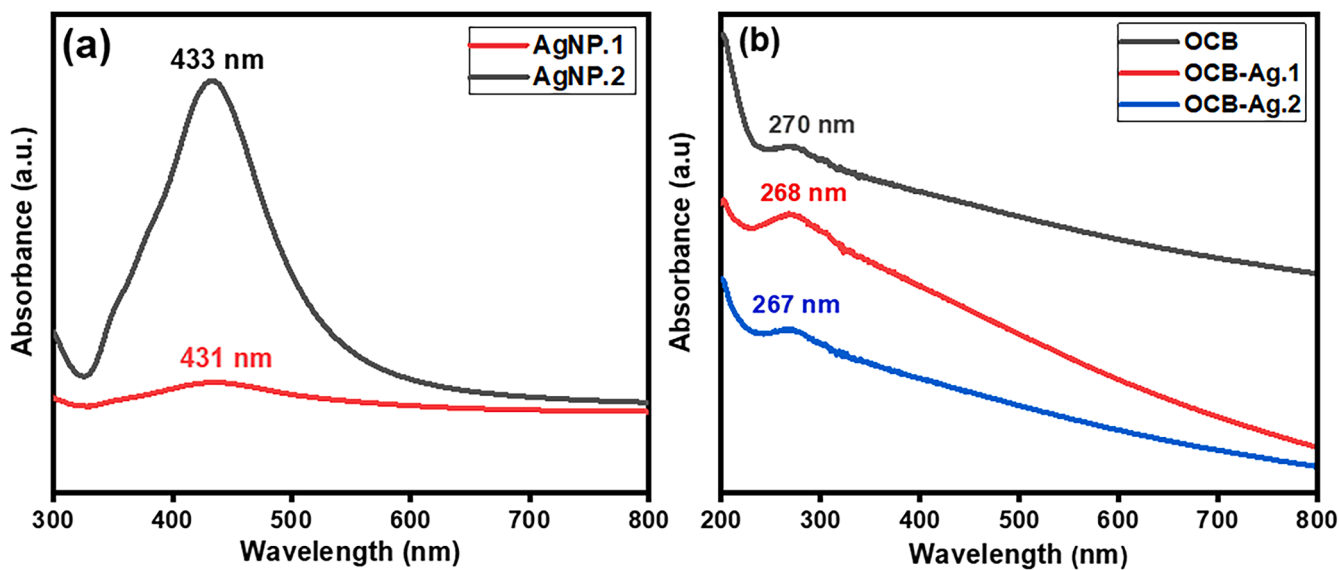


Fig. 5. (a) UV-Visible spectrum of AgNP.1 and AgNP.2 (b) UV-Visible Spectrum of OCB, OCB-Ag.1 and OCB-Ag.2.

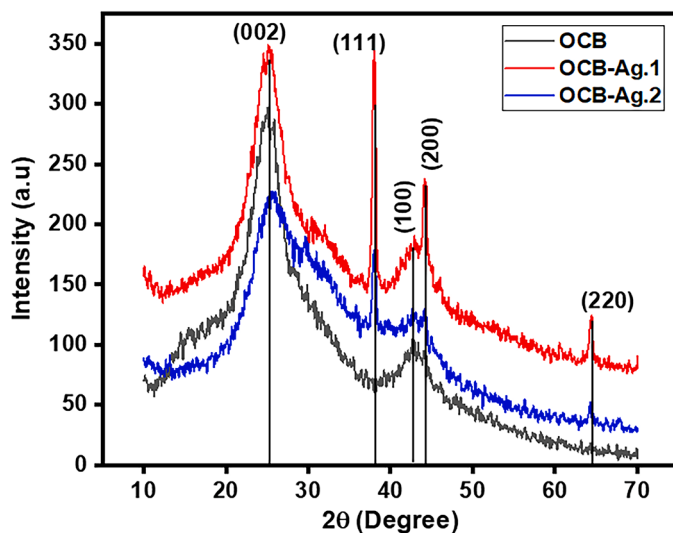


Fig. 6. XRD analysis of OCB and Ag embedded OCB (OCB-Ag.1 and OCB-Ag.2).

respectively. The size of composite is smaller than the bare OCB that may be attributed to the fact that the silver nanoparticles deposited into the pores of OCB and on its surface. The surface charges at the silver nanoparticles plausibly cause repulsion and thus improved the dispersion formation of OCB-Ag so as appeared smaller in size. As shown in Fig. 4(b) the zeta potential values for AgNP.1 and AgNP.2 are found to be -42 mV and -52 mV, while zeta potential values for OCB, OCB-Ag.1, and OCB-Ag.2 are -13.2 mV, -11.9 mV and -12.3 mV, respectively. The slight variation in the zeta potential value after composite formation represents that the stability of OCB was retained after incorporation of silver nanoparticles.

The presence of silver nanoparticles is also confirmed by using UV-Visible spectroscopy. The results from Fig. 5(a) indicated the appearance of absorption peak at 433 nm and 431 nm for the sample AgNP.1 and AgNP.2, respectively, which are the characteristics band for Ag nanoparticles. The increase in the concentration of trisodium citrate increases the concentration of citrate ions in the system, which readily encapsulates the silver nanoparticles and prevents them from aggregating together. Therefore, it is confirmed that the Ag nanoparticles are successfully synthesized using 1 % as well as 2 % of trisodium citrate. Fig. 5 (b) represents the UV- Visible spectrum of OCB and its composite with Ag. It is obvious that the absorption peak of silver disappeared in it, but characteristic absorption peak of OCB is appeared around 270 nm,

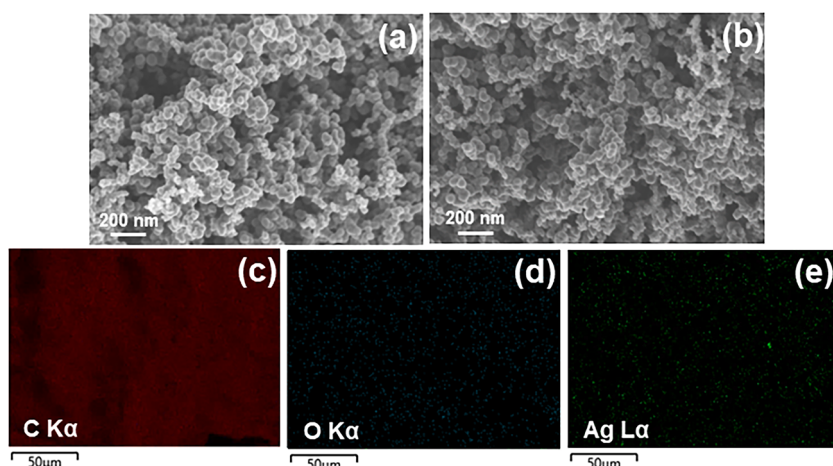


Fig. 7. SEM images of (a) OCB, (b) OCB-Ag, (c-e) EDS mapping of OCB-Ag sample.

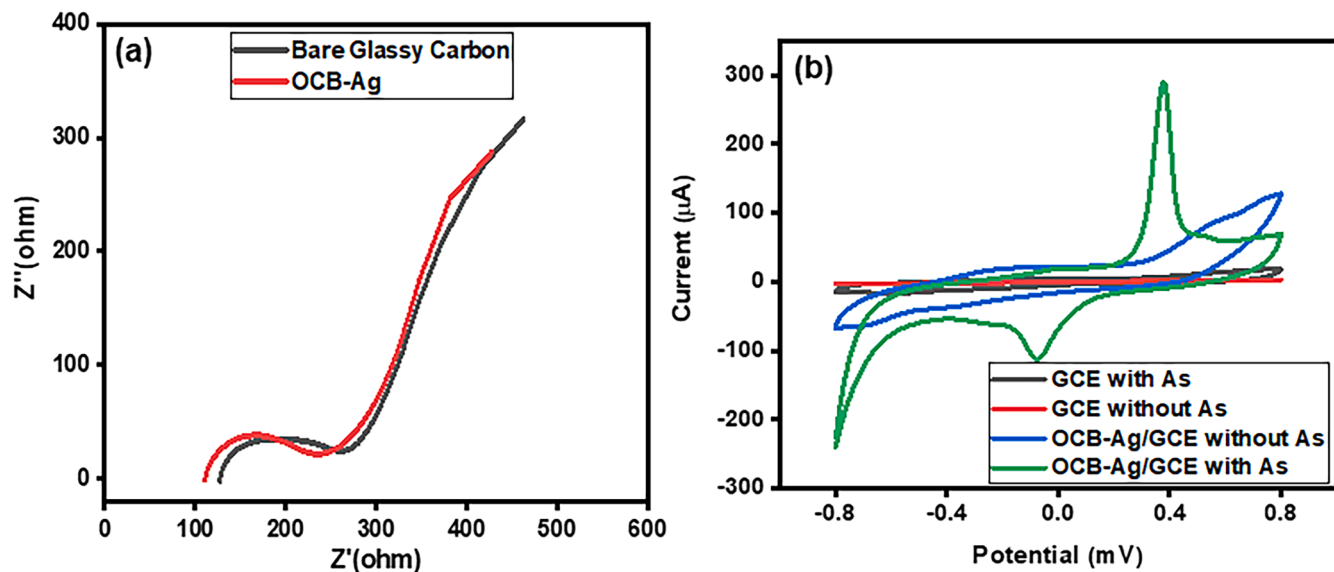


Fig. 8. (a) EIS in 0.1 M KCl containing 1.0 mM $\text{Fe}(\text{CN})_6 \text{K}_3$ (1: 1 mixture), (b) Cyclic Voltammetry of OCB-Ag/GCE in presence and absence of arsenic (50 ppm).

which slightly shifted to lower wavelength after deposition of Ag nanoparticles. This disappearance of absorbance signal for Ag nanoparticles could be attribute to the lower content of Ag, interaction of Ag and OCB substrate, or just higher absorbance of OCB that plausibly suppressed the Ag signal [34].

The XRD analysis of OCB and Ag embedded OCB (OCB-Ag.1 and OCB-Ag.2) is shown in Fig. 6. The diffraction peaks of OCB appeared at $2\theta = 25.18^\circ$ and 42.76° (JCPDS file No.75-1621) due to Bragg's reflections corresponding to (002) and (100) lattice planes. The diffraction angle (2θ) of the (002) peak of graphite is known to be 26.7° , but the (002) peak in Fig. 6 is located near 25.1° . This indicated that (002) peak shifted slightly due to oxidation of carbon. The peaks at $2\theta = 38.2^\circ$, 44.6° , 64.6° in composites (OCB-Ag.1 and OCB-Ag.2) are corresponding to (111), (200), (220) planes are observed. These peaks are matched with the face centered cubic (fcc) structure of silver (JCPDS file No. 04-0783) [35]. As the peak intensity of OCB-Ag.1 is higher than OCB-Ag.2, that might be due to reason that OCB-Ag.1 experiences size restricted penetration (because of their relatively greater size as appeared in Fig. 4(a) inside the OCB particles, which results in their greater presence onto the surface and thus provided the prominent signal in XRD).

Scherrer's equation was applied for the calculation of crystallite size of OCB and the Ag in the OCB-Ag.1 and OCB-Ag.2 composite. According to Scherrer's law, broader peaks correspond to small crystal sizes and also the broadening of the peaks evidences lower crystallinity [36]. The crystallite size for OCB, Ag in OCB-Ag.1 and Ag in OCB-Ag.2 were found as 0.7 nm, 7.1 nm and 1.6 nm, respectively. Based on the above results, it is attributed that the concentration of Ag nanoparticle is higher in OCB-Ag.2 sample. However, the crystallite size and particle size of the

Ag into OCB-Ag.2 composite is smaller that could lead to its higher surface area and thus could improve the sensing performance. It is also supported by the XRD results that the Ag is present in OCB-Ag composite prepared using 2 % trisodium citrate and is also well dispersed onto the OCB substrate. Therefore, OCB-Ag.2 is selected for further characterization and for evaluating the performance for As sensing, and for simplicity this sample will be denoted as OCB-Ag in subsequent part of this manuscript. The morphology of OCB-Ag is observed by scanning electron microscopy (SEM) as shown in Fig. 7(a) and (b). The SEM images indicated the spherical morphology of OCB, which retained as such after Ag nanoparticles embedding into it.

The sharp grain boundaries helped in the well dispersion of the OCB-Ag and that helped to form the superior quality electrode deposition

onto glassy carbon electrode through drop casting technique as used in this study. Since no change was observed in SEM images of OCB before and after embedding the AgNPs onto it, it was thus important to study the elemental composition of the OCB-Ag to ensure the presence of AgNPs in this sample. Thus, the EDS analysis of OCB-Ag was performed as shown in Fig. 7(c-e). The EDS results indicated the presence of carbon, oxygen and silver in OCB-Ag, which confirmed the existence of metallic AgNPs on the surface of OCB nanosheets. The presence of O also proved the successful oxidation of carbon black through the adopted procedure.

3.3. Electrochemical characterization of OCB-Ag

The working electrode was prepared by drop casting of OCB-Ag onto glassy carbon electrode and is designated as OCB-Ag/GCE. The electrochemical impedance spectroscopy (EIS) of OCB-Ag/GCE was carried out to determine the relative conductivity of electrode and charge transfer resistance behavior. EIS is a useful method for probing characteristics of surface-modified electrodes. The semicircle portion observed at high frequencies in the Nyquist plot corresponds to the charge transfer limiting process, and the charge transfer resistance (R_{ct}) values can be directly measured as the diameter of the semicircle. The EIS results in Fig. 8(a) show that the charge transfer resistance (R_{ct}) value of OCB-Ag/GCE is 165 ohm that is lower than the R_{ct} value of bare GCE that is 179 ohms, which is recorded in 1 mM $\text{Fe}(\text{CN})_6 \text{K}_3$ with 0.1 M KCl as the supporting electrolyte. This indicated the excellent electrical properties and high surface area of OCB and silver nanoparticles, which acts as a fast electron conduction pathway between the electrode and the electrochemical probe.

In order to investigate the electrocatalytic activity and redox response of prepared electrode for arsenic detection, the cyclic voltammetry is performed by using OCB-Ag/GCE as working electrode while using H_2SO_4 (0.1 M) as supporting electrolyte with and without arsenic in aqueous solution. Cyclic voltammetry was conducted to evaluate the response of the bare GCE both in the absence and presence of arsenic, as illustrated in Fig. 8(b). In both cases, the bare GCE showed no oxidation or reduction peaks. It is further indicated by Fig. 8(b) that there is no redox response observed in the absence of arsenic in the range of -0.8 to $+0.8$ V for OCB-Ag/GCE, while a strong oxidation as well as reduction peak is observed when the electrolyte solution contained arsenic. The oxidation peak is observed at 0.36 V (vs. Ag/AgCl) in forward scan and reduction peak is observed at -0.06 V (vs. Ag/AgCl) in reversed scan. Two different batches of OCB-Ag were prepared with the same method

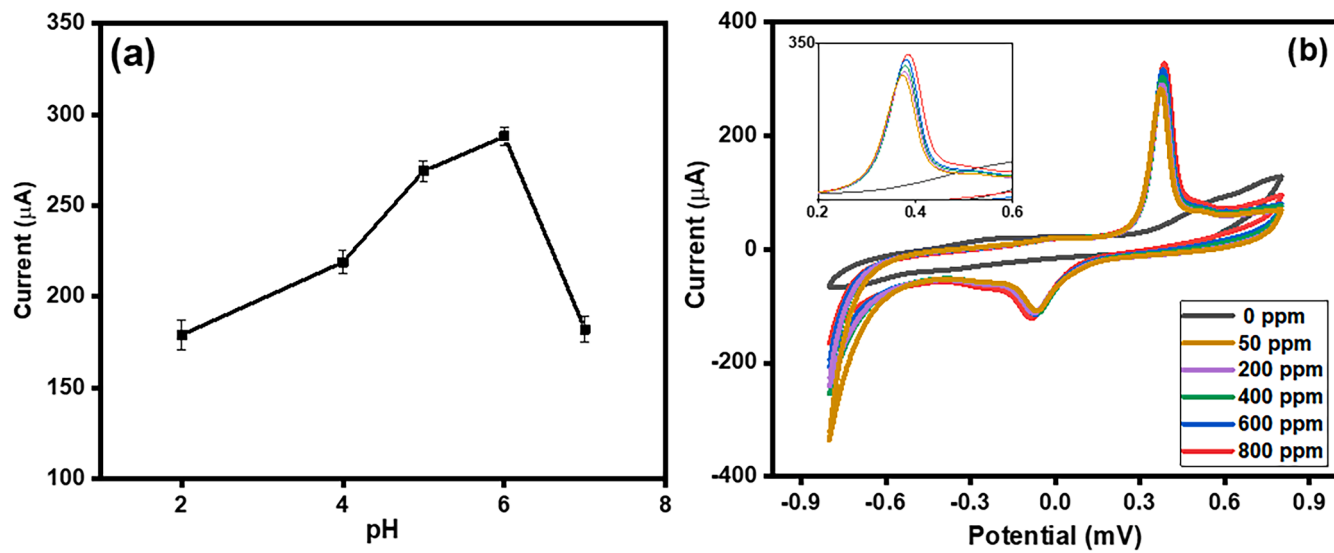


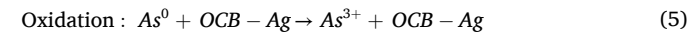
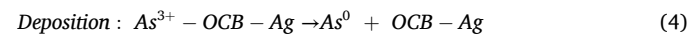
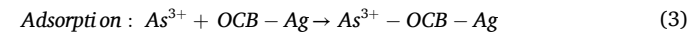
Fig. 9. (a) pH optimization study (b) Cyclic Voltammetry of OCB-Ag/GCE with increasing concentration of As^{3+} from 0 to 800 ppm at scan rate 50 mV sec^{-1} . (Error bars are based on measurement of each sample in triplicate).

and the sensing response was evaluated by cyclic voltammetry as presented in Fig. S1 to ensure the reproducibility of electrode material signal towards Arsenic. The Fig. S1 indicates that the current response for the sensing of As remained almost similar and at same potential value for both the samples. This strong oxidation and reduction signals are due to synergistic effect of Ag in combination with OCB. This combination provides excellent catalytic ability and a high surface area, leading to a significant response when interacting with arsenic in the solution. This interaction causes the strong bases of this platform to function as a sensor, a conclusion also corroborated by computational studies reported previously.

3.4. Possible mechanism for detection of As^{3+} an effect of pH

The feasible detection mechanism of As^{3+} ions on OCB-Ag is illustrated in Eqs. (3)-(5). The As^{3+} initially diffuses from solution to the electrode material and is adsorbed on the surface of OCB-Ag by coordinating with oxygenated functional groups on the nanocomposite, which attributes significant multilayer adsorption tendency. The

interaction occurred between As^{3+} and OCB-Ag followed by transformation of As^{3+} to As^0 through reduction process during preconcentration step and then deposited on the surface of electrode. After that the oxidation stripping signal of arsenic is captured by using positive potential. The oxidation of As over OCB-Ag is catalyzed by electrochemical pathway as shown in following Eqs. (3)-(5).



The detection of arsenic by OCB-Ag electrode material is strongly affected by the pH of solution. The results in Fig. 9(a) shows that the current response increases with increase of pH of solution and maximum current value reaches at pH 6. It can be explained as in the highly acidic conditions, the most prominent species of As^{3+} are protonated form having no charge as H_3AsO_3 . At low pH, due to excess of H^+ ions the equilibrium of reaction is disturbed, and tendency of reaction mixture is

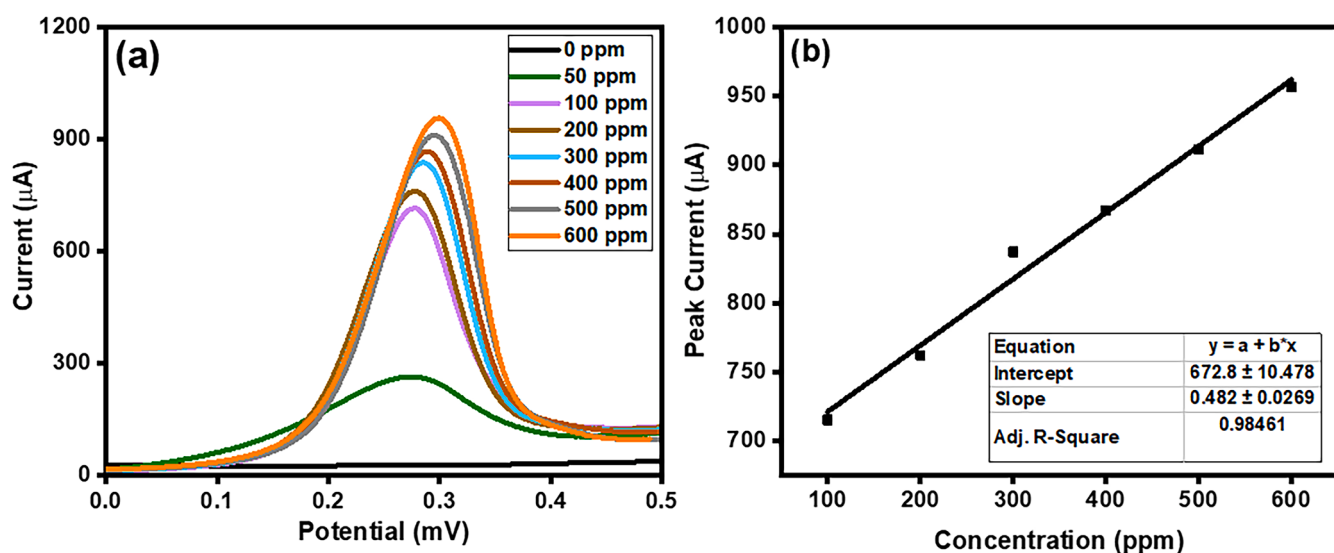


Fig. 10. (a) SW-ASV responses with respect to increasing As^{3+} concentration from 100 to 600 ppm, respectively in $0.1 \text{ M H}_2\text{SO}_4$. Deposition potential: 0.5 V for 2 min, rest period: 10 s, frequency: 40 Hz, pulse amplitude: 25 mV, (b) Calibration curve.

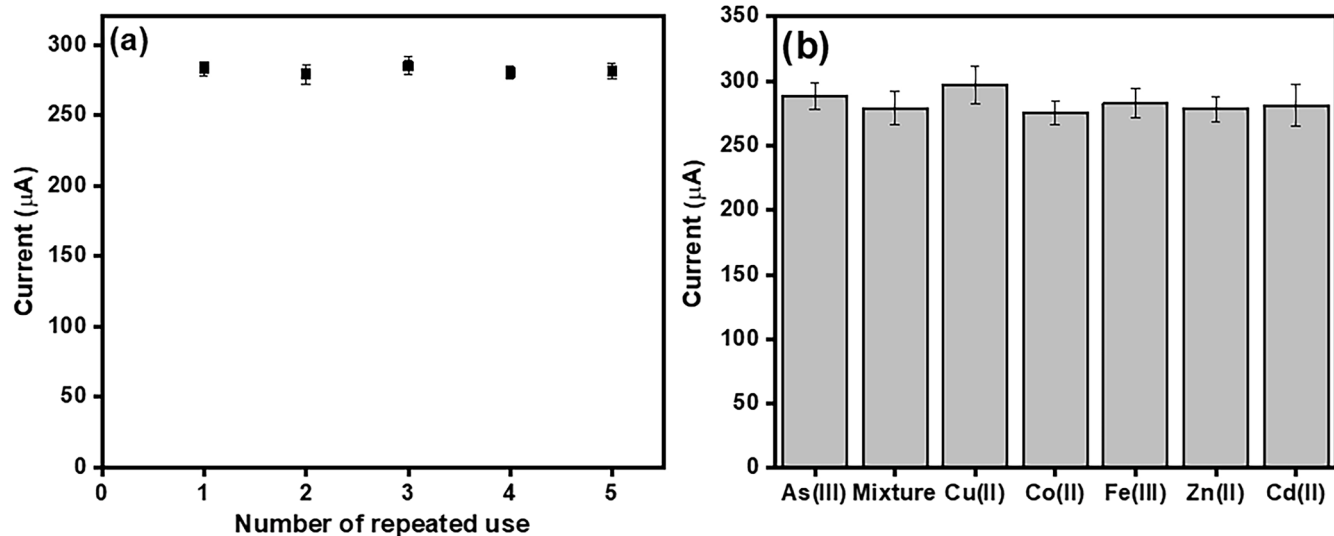


Fig. 11. (a) Repeatability response of OCB-Ag based sensing electrode (b) Interference study of competing ions at Voltage 0.278 (Error bars are based on measurement of each sample in triplicate).

more towards left side of reaction as shown in Eqs. (6)-(9), and the adsorption of the uncharged species at the electrode surface is lower than the charged one. When the pH of solution increases then limited H^+ ions will appear in reaction mixture because of H_3AsO_3 dissociation, thus arsenic species mostly exist in anionic form as $H_2AsO_3^-$, $HAsO_3^{2-}$ and AsO_3^{3-} . In addition, at low pH protonation occurs on the oxygen groups present on the surface of OCB-Ag, as a result low current response is produced. These anionic species interact with oxygen containing the relatively negatively charged surface of OCB. As a result, detection of As^{3+} occurred as adsorption followed by redox process i.e., conversion of As^{3+} to As^0 during reduction and oxidation As^0 to As^{3+} upon anodic stripping. At high pH, the competing phenomenon between OH^- and anionic species of arsenic occurred as a result current response decreases [37,38].



The detection of As^{3+} species having different concentrations that is 50–800 ppm were performed by using cyclic voltammetry as shown in Fig. 9(b). The results suggested that the same oxidation peak occurs at 0.36 V and reduction peak at –0.06 V.

3.5. Square wave anodic stripping voltammetry (SWASV)

The SWASV response of different concentration of As^{3+} at OCB-Ag were recorded under optimum experimental conditions as shown in Fig. 10(a). The optimum conditions were maintained such as frequency of 40 Hz, deposition potential –0.5 V, pulse amplitude of 25 mV and deposition time (time at which analyte deposit on the surface of electrode) is set as 2 min. Deposition time of about 2 min was used in SWASV for arsenic detection. Since the higher deposition time is required for detection of low concentration of analyte thus for uniformity in study 2 min are taken as deposition time for all analysis. The stripping peak current of As^{3+} increases gradually with increasing concentration of As^{3+} . It presents a good and linear relationship with As^{3+} concentration in the range of 100 to 600 ppm and the corresponding linear regression equation as $I = 0.48 (\text{mg L}^{-1}) + 672.80$ with regression coefficient is

found to be $R^2 = 0.985$ by drawing a calibration plot as shown in Fig. 10 (b).

The strong stripping peak of arsenic was observed at 0.278 V for different concentration of arsenic solution starting from 50 ppm to 600 ppm. It is observed all concentration of arsenic responded well and prominent signal appeared at particular potential with different peak current. Although, the signal for arsenic at concentration lower than 100 ppm is also observed but the linear range started from 100 ppm. The current response for arsenic concentration 50 ppm is also added in Fig. 10(a), but it was not taken as a linear range point for calibration curve. The linear range studied, where peak current is found to be directly proportional to the concentration of arsenic analyte. From the calibration plot of current vs. concentrations of As^{3+} Fig. 10(b), the limit of detection (LOD), limit of quantification (LOQ), and sensitivity of the OCB-Ag sensing platform were estimated to be 0.01 ppm, 0.1 ppm, and $5.9 \mu\text{A ppm}^{-1}$, respectively.

3.6. Repeatability and interference study

The frequent problem that is encountered by the sensing materials during the detection of analyte is their instability and poor recovery upon repeated use. Five measurements were conducted using prepared OCB-Ag nanocomposite for arsenic detection and just a slight drop of current is observed as shown in Fig. 11(a). The results suggested that the developed electrode material exhibited the standard deviation of 0.84 after consecutive 5 sensing measurements. Another obstacle against the accurate detection of As^{3+} in an aqueous solution is the co-presence of various metal ions including Cu^{2+} , Co^{2+} , Zn^{2+} , Fe^{2+} and Cd^{2+} . The presence of coexisting ions in the sample leads to interference if they co-deposit and subsequently strip away at the same potential values as applied for arsenic. To assess the interference caused by these metal ions, experiments were conducted using a concentration of 100 ppm for each ion in a 50 ppm As^{3+} solution. The lower concentration of arsenic is selected due to the reason that if the lower concentration detection is not interfered with by other species in the system, then it could be assumed that the interference will be even less prominent in higher concentration.

The Cu^{2+} is one of the common interfering species as compared to other ions because the stripping potential of Cu^{2+} is very closed to As^{3+} and it can co-deposit with As^{3+} and form intermetallic bond during detection process [38]. The results shown in Fig. 11(b) indicated that although not significant but still the presence of Cu^{2+} has some impact

Table 2Comparison of OCB-Ag with different types of materials used for electrochemical detection of arsenic (As^{3+}) from waste water.

Types of modified electrode	Electrochemical Technique	LOD (ppm)	Sensitivity ($\mu\text{A}\cdot\text{ppm}^{-1}$)	Linear range (ppm)	Ref.
OCB-Ag	SWASV	0.01	5.90	100–600	present work
Ag-MT NCs	DPASV	38.2	0.02953	10–300	[40]
rGO/Ag	DPAVs	0.00024	0.00124	0–0.025	[41]
Au NPs modified carbon	SWASV	0.0167	0.0001	0–0.150	[42]
Au/GO/Leucine	CV	30	5–50	0.5	[43]
Au- carbon nanosheets	CV	0.0001	–	0.0001–100	[44]
Fe-Chitosan	SWASV	0.00112	3.66	0–0.025	[45]
Ag@SiO ₂ /PANI NFS	SWASV	0.013	0.83	0.1–100	[46]

on the detection signal of As^{3+} , and this effect is likely due to the formation of intermetallic compounds that enhance the deposition of As^{3+} during the cathodic deposition. The analysis of other ions was performed by using the same concentration for As^{3+} and 100 ppm of each of other metal ion. In solutions containing varying interfering ions, there is no significant peak variation observed, with no meaningful change occurring in the current response generated for As^{3+} even with the concentrations of the interference ions are 2 times more than that of As^{3+} (Fig. 11(b)). This suggests that these ions including Cu^{2+} do not substantially interfere with the detection of As^{3+} step using the developed OCB-Ag sensing platform [39].

Various analytical parameters including electrolyte, measurement technique, detection range, sensitivity and LOD for the prepared OCB-Ag/GC electrode are compared with some of the relevant and recently reported literature that is summarized in Table 2. Although the synthesis of OCB-Ag is facile and the material used are cost effective but the detection limit, linear calibration range and sensitivity for arsenic determination at this modified electrode are comparable to those obtained by using other modified carbon based electrodes in combination with metal nanoparticles.

This study introduces avenues for designing effective sensing platforms through the integration of Density Functional Theory (DFT) studies with experimental validation. DFT enables the exploration of various materials to pinpoint those with optimal interactions with the analyte, thereby saving time and resources by identifying promising materials for further experimental investigation. This research approach advocates for future researchers to integrate theoretical and experimental work more closely, aiming to design and enhance sensor efficiency. Such a collaborative approach extends beyond sensor design, encompassing fields like electrochemical energy storage and electrocatalysis, thus contributing to advancements in these areas of research.

4. Conclusion

DFT approach is successfully applied to successfully designs Ag embedded OCB sensing platform for As detection. Theoretical analysis proves Ag incorporation enhances OCB performance in arsenic sensing. Ag embedding improves conductivity and interaction of OCB-Ag with arsenic, shown by repositioning of HUMO and LUMO, higher interaction energy ($E_{\text{int}} = -1.996 \text{ eV}$), and low energy gap ($E_{\text{H-L}} = 0.45 \text{ eV}$). This design is experimentally validated. OCB-Ag exhibits lowest charge transfer resistance ($R_{\text{ct}}=165 \text{ ohm}$), indicating excellent electrical properties and high surface area. Strong oxidation and reduction peak in Cyclic Voltammetry is due to synergistic effect of Ag and OCB, providing good catalytic ability and response time to arsenic. OCB-Ag sensor shows linear current response from 100 ppm to 600 ppm of As^{3+} . Limit of detection is found to be 0.01 ppm that is also within the permissible limit set by world health organization. Limit of quantification and sensitivity achieved are 0.1 ppm and $5.9 \mu\text{A}\cdot\text{ppm}^{-1}$, respectively. Interference study confirmed OCB-Ag selectivity towards arsenic detection. The OCB-Ag is a cost-effective material prepared through facile synthesis and proved to be a potential candidate for arsenic sensing. Moreover, the DFT is found to be a useful technique to design and predict the material suitability for

sensing application. This approach can be extended to devise materials for various advanced applications while promoting energy, resource, and environmental conservation.

CRediT authorship contribution statement

Aneeqa Batool: Writing – original draft, Software, Methodology, Investigation, Formal analysis, Conceptualization. **Sana Qureshi:** Software, Methodology, Investigation, Formal analysis, Conceptualization. **Arslan Ahmad:** Writing – original draft, Software, Methodology, Formal analysis, Conceptualization. **Shaista Zubaid:** Writing – review & editing, Software, Methodology, Formal analysis. **Laraib Saeed:** Software, Methodology, Formal analysis. **Khurshid Ayub:** Visualization, Validation, Software. **Tahir Rasheed:** Validation, Software, Methodology. **Tauqir A. Sherazi:** Writing – review & editing, Visualization, Validation, Supervision, Resources, Project administration, Funding acquisition, Conceptualization.

Declaration of competing interest

The authors declare that they have no known competing financial interests or personal relationships that could have appeared to influence the work reported in this paper.

Data availability

Data will be made available on request.

Acknowledgement

Tauqir A. Sherazi acknowledges the financial support from the Alexander von Humboldt Foundation. The authors are grateful to the Pakistan Science Foundation (PSF/NSFC-Eng/KP-COMSATS-ABT-04) and the Higher Education Commission of Pakistan (20-3684/R&D/HEC/14) for financial support. The authors kindly acknowledge Dr. Faizan Ullah and Mr. Muhammad Aetizaz (both from Department of Chemistry, COMSATS University Islamabad, Abbottabad Campus) for their input in DFT studies.

Supplementary materials

Supplementary material associated with this article can be found, in the online version, at [doi:10.1016/j.surfin.2024.104843](https://doi.org/10.1016/j.surfin.2024.104843).

References

- [1] J. Podgorski, M. Berg, Global threat of arsenic in groundwater, *Science* 368 (6493) (2020) 845–850.
- [2] M. Kumareshan, P. Riyazuddin, Overview of speciation chemistry of arsenic, *Curr. Sci.* 80 (2001) 837–846.
- [3] L. Del Razo, M. Arellano, M. Cebrian, The oxidation states of arsenic in well-water from a chronic arsenicism area of northern Mexico, *Environ. Pollut.* 64 (2) (1990) 143–153.

- [4] A.H. Smith, E.O. Lingas, M. Rahman, Contamination of drinking-water by arsenic in Bangladesh: a public health emergency, *Bull. World Health Organ.* 78 (9) (2000) 1093–1103.
- [5] M. Kononenko, W.H. Frishman, Association between arsenic exposure and cardiovascular disease, *Cardiol. Rev.* 29 (4) (2021) 217–221.
- [6] H.G. Gorchev, G. Ozolins, WHO guidelines for drinking-water quality, *WHO chron* 38 (3) (1984) 104–108.
- [7] E. Byeon, H.-M. Kang, C. Yoon, J.-S. Lee, Toxicity mechanisms of arsenic compounds in aquatic organisms, *Aquat. Toxicol.* 237 (2021) 105901.
- [8] A. Bhat, T.O. Hara, F. Tian, B. Singh, Review of analytical techniques for arsenic detection and determination in drinking water, *Env. Sci., Adv.* 2 (2) (2023) 171–195.
- [9] Q. Ding, C. Li, H. Wang, C. Xu, H. Kuang, Electrochemical detection of heavy metal ions in water, *Chem. Comm.* 57 (59) (2021) 7215–7231.
- [10] W. Qian, B. Hong-Mei, H. Xiao-Jun, Research progress of electrochemical detection of heavy metal ions, *Chinese J. Anal. Chem.* 49 (3) (2021) 330–340.
- [11] V. Mirceski, R. Gulaboski, M. Lovric, I. Bogeski, R. Kappl, M. Hoth, Square-wave voltammetry: a review on the recent progress, *Electroanalysis* 25 (11) (2013) 2411–2422.
- [12] N. Raj, R.M. Crooks, Detection Efficiency of Ag Nanoparticle Labels for a Heart Failure Marker Using Linear and Square-Wave Anodic Stripping Voltammetry, *Biosensors* 12 (4) (2022) 203.
- [13] Y. Lu, X. Liang, C. Niyungeko, J. Zhou, J. Xu, G. Tian, A review of the identification and detection of heavy metal ions in the environment by voltammetry, *Talanta* 178 (2018) 324–338.
- [14] R. Ramachandran, T.-W. Chen, S.-M. Chen, T. Baskar, R. Kannan, P. Elumalai, P. Raja, T. Jeyapragasam, K. Dinakaran, A review of the advanced developments of electrochemical sensors for the detection of toxic and bioactive molecules, *Inorg. Chem. Front.* 6 (12) (2019) 3418–3439.
- [15] A. Batool, T.A. Sherazi, S.A.R. Naqvi, *Organic-Inorganic Nanohybrid-Based Electrochemical Biosensors, Hybrid Nanomaterials: Biomedical, Environmental and Energy Applications*, Springer, 2022, pp. 151–173.
- [16] B. Bansod, T. Kumar, R. Thakur, S. Rana, I. Singh, A review on various electrochemical techniques for heavy metal ion detection with different sensing platforms, *Biosens. Bioelectron.* 94 (2017) 443–455.
- [17] R. Rajeev, R. Datta, A. Varghese, Y. Sudhakar, L. George, Recent advances in bimetallic based nanostructures: synthesis and electrochemical sensing applications, *Microchem. J.* 163 (2021) 105910.
- [18] D. Ayodhya, Recent progress on detection of bivalent, trivalent, and hexavalent toxic heavy metal ions in water using metallic nanoparticles: a review, *Results Chem* 5 (2023) 100874.
- [19] A. Sabir, T.A. Sherazi, Q. Xu, Porous polymer supported Ag-TiO₂ as green photocatalyst for degradation of methyl orange, *Surf. Interfaces* 26 (2021) 101318.
- [20] I. Ivanović, The role of silver nanoparticles in electrochemical sensors for aquatic environmental analysis, *Sensors* 23 (7) (2023) 3692.
- [21] F. Arduini, S. Cinti, V. Mazzaracchio, V. Scognamiglio, A. Amine, D. Moscone, Carbon black as an outstanding and affordable nanomaterial for electrochemical (bio) sensor design, *Biosens. Bioelectron.* 156 (2020) 112033.
- [22] M. Alam, M. Islam, M. Mina, M. Gafur, Structural, mechanical, thermal, and electrical properties of carbon black reinforced polyester resin composites, *J. Appl. Polym. Sci.* 131 (13) (2014).
- [23] J.P. Chen, S. Wu, Acid/base-treated activated carbons: characterization of functional groups and metal adsorptive properties, *Langmuir* 20 (6) (2004) 2233–2242.
- [24] X.-W. Chen, Y.-S. Chen, X.-M. Ding, L. Wang, J. Liu, R.-F. Wang, Rapid detection of tyrosinase in shrimp by polyacid-based electrochemical sensors, *Tungsten* 5 (1) (2023) 81–90.
- [25] S. Kaviani, D.A. Tayurskii, O.V. Nedopekin, I. Piyaznina, DFT insight into Cd²⁺, Hg²⁺, Pb²⁺, Sn²⁺, As³⁺, Sb³⁺, and Cr³⁺ heavy metal ions adsorption onto surface of bowl-like B30 nanosheet, *J. Mol. Liq.* 365 (2022) 120131.
- [26] M. Khnifira, W. Boumya, J. Attarki, A. Mabsoune, M. Sadiq, M. Abdennouri, S. Kaya, N. Barka, A combined DFT, Monte Carlo, and MD simulations of adsorption study of heavy metals on the carbon graphite (111) surface, *Chem. Phys. Impact* 5 (2022) 100121.
- [27] M. Frish, G. Trucks, H. Schlegel, G. Scuseria, M. Robb, J. Cheeseman, G. Scalmani, V. Barone, B. Mennucci, G. Paterson, Gaussian 09, Revision A. 02, Gaussian Inc, Wallingford CT, 2009.
- [28] S. Sarfaraz, M. Yar, A.A. Khan, R. Ahmad, K. Ayub, DFT investigation of adsorption of nitro-explosives over C2N surface: highly selective towards trinitro benzene, *J. Mol. Liq.* 352 (2022) 118652.
- [29] T. Lu, F. Chen, Multiwfns: a multifunctional wavefunction analyzer, *J. Comput. Chem.* 33 (5) (2012) 580–592.
- [30] W. Humphrey, A. Dalke, K. Schulter, VMD: visual molecular dynamics, *J. Mol. Graph.* 14 (1) (1996) 33–38.
- [31] A. Khan, T.A. Sherazi, Y. Khan, S. Li, S.A.R. Naqvi, Z. Cui, Fabrication and characterization of polysulfone/modified nanocarbon black composite antifouling ultrafiltration membranes, *J. Membr. Sci.* 554 (2018) 71–82.
- [32] Y. Zhang, Y. Zhao, Y. Yang, P. Liu, J. Liu, J. Zhang, DFT study on Hg0 adsorption over graphene oxide decorated by transition metals (Zn, Cu and Ni), *Appl. Surf. Sci.* 525 (2020) 146519.
- [33] T. Jadoon, T. Mahmood, K. Ayub, Silver-graphene quantum dots based electrochemical sensor for trinitrotoluene and p-nitrophenol, *J. Mol. Liq.* 306 (2020) 112878.
- [34] T. Swathy, M.J. Antony, Tangled silver nanoparticles embedded polythiophene-functionalized multiwalled carbon nanotube nanocomposites with remarkable electrical and thermal properties, *Polymer (Guildf)* 189 (2020) 122171.
- [35] A.S. Lanje, S.J. Sharma, R.B. Pode, Synthesis of silver nanoparticles: a safer alternative to conventional antimicrobial and antibacterial agents, *J. Chem. Pharm. Res* 2 (3) (2010) 478–483.
- [36] C. Alegre, M.E. Gálvez, R. Moliner, M.J. Lázaro, Influence of the synthesis method for Pt catalysts supported on highly mesoporous carbon xerogel and vulcan carbon black on the electro-oxidation of methanol, *Catal. 5 (1)* (2015) 392–405.
- [37] M. Baghayeri, M. Ghanei-Motlagh, R. Tayebi, M. Fayazi, F. Narenji, Application of graphene/zinc-based metal-organic framework nanocomposite for electrochemical sensing of As (III) in water resources, *Anal. Chim. Acta* 1099 (2020) 60–67.
- [38] P. Xiao, G. Zhu, X. Shang, B. Hu, B. Zhang, Z. Tang, J. Yang, J. Liu, An Fe-MOF/MXene-based ultra-sensitive electrochemical sensor for arsenic (III) measurement, *J. Electroanal. Chem.* 916 (2022) 116382.
- [39] M.C. Maridevaru, R. Kaimal, A.H. Naceruddin, B. Aljafari, S. Anandan, Nanotextured La0.95Ce0.05MnO3/GCE assemblage for ultrasensitive and precise electrochemical detection of arsenic (III) at neutral pH, *Surf. Interfaces* 34 (2022) 102359.
- [40] M.M. Dessie, A.A. Tsegaye, Silver nanoparticles incorporated local montmorillonite clay modified carbon paste electrode for the voltammetric determination of Arsenic (III) in aqueous solution, *Ethiop. J. Sci. Technol.* 16 (3) (2023) 209–224.
- [41] M.Y. Pabel, S. Yasmin, M.A.A. Shaikh, M.H. Kabir, Electronic waste derived reduced graphene oxide supported silver nanoparticles for the electrochemical sensing of trace level arsenite in aqueous medium, *Sensor and Actuat. A-Phys.* 366 (2024) 115028.
- [42] C. Sullivan, D. Lu, A. Senecal, P. Kurup, Voltammetric detection of arsenic (III) using gold nanoparticles modified carbon screen printed electrodes: application for facile and rapid analysis in commercial apple juice, *Food Chem* 352 (2021) 129327.
- [43] S. Kumar, G. Bhanjana, N. Dilbaghi, R. Kumar, A. Umar, Fabrication and characterization of highly sensitive and selective arsenic sensor based on ultra-thin graphene oxide nanosheets, *Sens. Actuators B: Chem.* 227 (2016) 29–34.
- [44] O. Agrawal, K. Saxena, U. Jain, N. Chauhan, H.K. Sharma, M. Balal, S.R. Barman, S. Das, M. Mukherjee, Carbon Nanosheets Infused with Gold Nanoparticles as an Ultrasensitive Nose for Electrochemical Arsenic Sensing, *ACS Omega* 8 (50) (2023) 48360–48369.
- [45] J.-H. Hwang, P. Pathak, X. Wang, K.L. Rodriguez, J. Park, H.J. Cho, W.H. Lee, A novel Fe-Chitosan-coated carbon electrode sensor for in situ As (III) detection in mining wastewater and soil leachate, *Sens. Actuators B: Chem.* 294 (2019) 89–97.
- [46] T. Feng, K. Chen, J. Zhong, Y. Cheng, H. Zhao, M. Lan, In-situ polymerization of dendritic polyaniline nanofibers network embedded with Ag@ SiO₂ core-shell nanoparticles for electrochemical determination of trace arsenic (III), *Sens. Actuators B: Chem.* 369 (2022) 132265.